GPS Solut (2013) 17:439–451
DOI 10.1007/s10291-013-0332-x

REVIEW ARTICLE

GLONASS pseudorange inter-channel biases and their effects on combined GPS/GLONASS precise point positioning

Shi Chuang · Yi Wenting · Song Weiwei · Lou Yidong · Yao yibin · Zhang Rui

Received: 16 October 2012 / Accepted: 18 June 2013 / Published online: 19 July 2013

Abstract Combined GPS/GLONASS precise point positioning (PPP) can obtain a more precise and reliable position than GPS PPP. However, because of frequency division multiple access, GLONASS carrier phase and pseudorange observations suffer from inter-channel biases (ICBs) which will influence the accuracy and convergence speed of combined GPS/GLONASS PPP. With clear understanding of the characteristics of carrier phase ICBs, we estimated undifferenced GLONASS pseudorange ICBs for 133 receivers from five manufacturers and analyzed their characteristics. In general, pseudorange ICBs corresponding to the same firmware have strong correlations. The ICB values of two receivers with the same firmware may be different because of different antenna types, and their differences are closely related to frequency. Pseudorange ICBs should be provided for each satellite to obtain more precise ICBs as the pseudorange ICBs may vary even on the same frequency. For the solutions of standard point positioning (SPP), after pseudorange ICB calibration, the mean root mean square (RMS) improvements of GLONASS SPP reach up to 57, 48, and 53 % for the East, North, and Up components, while combined GPS/GLONASS SPP reach up to 27, 17, and 23 %, respectively. The combined GPS/GLONASS PPP after pseudorange ICB calibration evidently improved the convergence speed, and the mean RMS of PPP improved by almost 50 % during the convergence period.

S. Chuang · Y. Wenting · S. Weiwei (✉) · L. Yidong · Z. Rui
Research Center of GNSS, Wuhan University, 129 Luoyu Road, Wuhan 430079, China
e-mail: SWW@whu.edu.cn

Y. yibin · Z. Rui
School of Geodesy and Geomatics, Wuhan University, Wuhan 430079, China

Keywords GLONASS · GPS · Inter-channel bias · Pseudorange · PPP

Introduction

Precise point positioning (PPP) mainly using global positioning system (GPS) measurements achieves accuracy for static and mobile receivers at the millimeter to decimeter levels, respectively (Zumberge et al. 1997; Bisnath and Gao 2008). Combined GPS/GLONASS PPP has become increasingly popular with the revival of GLONASS. However, the GLONASS carrier phase and pseudorange observations suffer from inter-channel biases (ICBs) because the signal structure of GLONASS is based on a frequency division multiple access (Wanninger and Wallstab-Freitag 2007). Many studies proved that carrier phase ICBs are linear functions of frequency and that GLONASS ambiguities can be fixed by calibrating phase observations using a linear model (Kozlov and Tkachenko 1998; Rossbach and Hein 1996; Zinoviev 2005; Wanninger and Wallstab-Freitag 2007; Yamanda et al. 2010; Al-Shaery et al. 2012; Wanninger 2012). A few studies estimated the pseudorange ICBs of several GPS/GLONASS receivers using short baseline data, and the results indicated that pseudorange ICBs can reach up to several meters (Tsujii et al. 2000; Yamanda et al. 2010; Al-Shaery et al. 2012). However, these studies did not analyze the characteristics of pseudorange ICBs. Kozlov et al. (2000) analyzed the characteristics of GG24, GG12, and Z18 receiver pseudorange ICBs and proved that these ICBs are independent of receiver pairs and stable over time. Unfortunately, different from carrier phase ICBs, pseudorange ICBs have no obvious pattern of magnitude with frequency, though it is expected for some receivers to have larger biases for edge frequencies.

Wanninger (2012) estimated GLONASS differential carrier phase ICBs based on the data of 133 individual GPS/GLONASS receivers and analyzed their characteristics. However, he did not include pseudorange ICBs. Estimating and analyzing pseudorange ICBs are necessary because of their importance to PPP, especially in the ambiguity resolution for a single receiver. To enable PPP ambiguity resolution, the Melbourne-Wubbena combination observations have to be used to estimate wide-lane fractional-cycle biases, which are affected by pseudorange ICBs (Ge et al. 2008; Geng et al. 2010a, b, 2012). Therefore, a close investigation on the characteristics of pseudorange ICBs is critical in the implementation of GLONASS PPP ambiguity resolution. We estimate GLONASS undifferenced pseudorange ICBs and analyze them for 133 individual GPS/GLONASS receivers produced by five manufacturers. The stability of these ICBs over time and the relationships of pseudorange ICBs to receiver firmware version, antenna type, and frequency were determined. However, this study does not show the relationship between receiver type and pseudorange ICBs because these ICBs vary with receiver types. Furthermore, we compared the solutions of standard point positioning (SPP), as well as PPP, before and after pseudorange ICB calibration. Standard point positioning, in this study, is defined as positioning using only pseudorange observations along with precision orbit and clock products. The ionospheric-free combination is used.

Determination of code ICBs

Global positioning system and GLONASS undifferenced pseudorange and carrier phase observations can be described as

$$\begin{aligned} P^{\mathrm{SYS},i} &= \rho^i + c(\mathrm{d}t^i - \mathrm{d}T) + I^i + m^i T + b^i + \varepsilon\left(P^{\mathrm{SYS},i}\right) \\ \Phi^{\mathrm{SYS},i} &= \rho^i + c(\mathrm{d}t^i - \mathrm{d}T) - I^i + m^i T + \lambda^i N^i + B^i + \varepsilon\left(\Phi^{\mathrm{SYS},i}\right) \end{aligned} \tag{1}$$

where the superscript SYS refers to the GPS or GLONASS system, the superscript i refers to a satellite, $P^{\mathrm{SYS},\ i}$ is the pseudorange observation, $\phi^{\mathrm{SYS},i}$ is the carrier phase observation, ρ^{i} is the range from satellite to receiver, c is the speed of light in vacuum, $\mathrm{d}t^i$ is the satellite clock bias, $\mathrm{d}T$ is the receiver clock bias, I^i is the ionosphere delay, m^i is the tropospheric mapping function, T is the zenith troposphere delay, λ^i is the signal wavelength, N^i is the integer carrier phase ambiguity, b^i is the pseudorange ICB, B^i is the carrier phase ICB, and $\varepsilon(P^{\mathrm{SYS},\ i})$ and $\varepsilon(\phi^{\mathrm{SYS},\ i})$ represent the observation noise.

In combined GPS/GLONASS PPP, the ICBs are absent for GPS (Kozlov et al. 2000), and GLONASS carrier phase ICBs are usually ignored if the ambiguities are not fixed because they can be absorbed by the ambiguities. However, the GLONASS pseudorange ICBs vary with each satellite. If improperly modeled, pseudorange ICBs cannot be absorbed completely by receiver clocks and remaining residual biases degrade the positioning accuracy. Assuming that the GLONASS pseudorange ICBs do not change within 24 h, we estimated the receiver GLONASS pseudorange ICBs using the undifferenced PPP approach based on GPS pseudorange, carrier phase, and GLONASS pseudorange observations. GLONASS carrier phase observations are not used because they are unnecessary for pseudorange ICB estimation.

To eliminate the impacts of systematic errors, we used the final orbits and clocks released by the European Space Agency, which provided both GPS and GLONASS precise orbits and clock bias. Moreover, we fixed the station coordinates to the true values and formed the ionosphere-free combinations to eliminate first-order ionospheric effects. The dry components of the troposphere, solid earth tides, Sagnac delay, etc., were corrected using high-precision models, whereas the wet components of the troposphere were estimated by the random walk method. Therefore, the ionosphere-free combinations observations can be written as

$$\begin{aligned} P_{\mathrm{ion},k}^{\mathrm{GPS},i} &= c\mathrm{d}T_k^{\mathrm{GPS}} + m_k^i T_k^w + \varepsilon\left(P_{\mathrm{ion},k}^{\mathrm{GPS},i}\right) \\ \Phi_{\mathrm{ion},k}^{\mathrm{GPS},i} &= c\mathrm{d}T_k^{\mathrm{GPS}} + m_k^i T_k^w + \lambda^i N_k^i + \varepsilon\left(\Phi_{\mathrm{ion},k}^{\mathrm{GPS},i}\right) \\ P_{\mathrm{ion},k}^{\mathrm{GLO},j} &= c\mathrm{d}T_k^{\mathrm{GLO}} + m_k^j T_k^w + b_k^j + \varepsilon\left(P_{\mathrm{ion},k}^{\mathrm{GLO},j}\right) \end{aligned} \tag{2}$$

where the subscript ion refers to ionosphere-free combination observations, the subscript k refers to a station, and T_k^w is the wet component of the zenith tropospheric delays of station k.

The receiver GLONASS clock bias and pseudorange ICBs in (2) are strongly correlated. To separate them from each other, we constrained the pseudorange ICBs as

$$\frac{1}{24}\sum_{j=1}^{24} b_k^j = 0 \tag{3}$$

Using this approach, we can estimate the daily pseudorange ICBs for each station. However, the ICBs actually contain the effects of satellite and Analysis Center (AC)-specific clock biases. To analyze the characteristics of the pseudorange ICBs, we still need to separate these specific clock biases from the pseudorange ICBs. Considering that these specific clock biases have the same impacts on all stations (Leos Mervart and Georg Weber 2011), we can separate them by subtracting the common parts of pseudorange ICBs estimations in all stations. So the pure pseudorange ICBs are

$$b_k^j = \hat{b}_k^j - \frac{1}{m}\sum_{k=1}^{m} \hat{b}_k^j \quad (4)$$

where m is number of stations, $\hat{b}_k^j$ is the daily pseudorange ICB estimates which contain the effects of satellite and AC specific clock biases.

Data processing and discussion

The data from 133 International GNSS Service (IGS) stations were used to estimate the GLONASS pseudorange ICBs. Considering that GLONASS was a full constellation of 24 satellites on December 8, 2011 (IAC, http://www.glonass-center.ru/en), we selected the data from day of year (DoY) 1 to DoY 136 in 2012. The receiver types and the number of individual receivers are listed in Table 1.

Stability of pseudorange ICBs

Figure 1 shows the time series of pseudorange ICB valuations for stations NANO, FRDN, ZIM2, and BRST. This figure depicts the changes in pseudorange ICBs over time. The receiver types and firmware versions which are obtained from the RINEX file headers are listed in Table 2.

From DoY 1 to DoY 136 in 2012, the firmware version for station NANO was not updated, and the pseudorange ICB valuations are seen to be very stable. However, the firmware version of stations FRDN and ZIM2 was updated on DoY 68 and 121 in 2012, respectively. The pseudorange ICB estimates of R02 and R03 in station FRDN evidently jumped when the firmware was updated, whereas the pseudorange ICB estimates in station ZIM2 did not change much. A total of 21 stations had updated firmware, and eight stations had pseudorange ICB valuations that evidently jumped. Moreover, when the antenna type at station BRST was updated, the pseudorange ICB valuations of R02 and R03 jumped.

Table 1 GPS/GLONASS receiver types and numbers of individual receivers used in this study

Manufacturer	Receiver type	Number of stations
JAVAD	TRE_G3TH DELTA	10
JPS	E_GGD	3
	EGGDT	12
	LEGACY	10
LEICA	GRX1200 + GNSS	10
	GRX1200GGPRO	32
TPS	E_GGD	4
	NETG3	11
	NET-G3A	6
TRIMBLE	NETR5	20
	NETR9	15
SUM	–	133

We also calculated the standard deviations of the daily pseudorange ICB estimates for each satellite. As the daily pseudorange ICB estimates may jump, in this case, the standard deviations of the daily pseudorange ICB estimates before and after the jump were calculated independently. The average standard deviation of the 24 satellites for each station was obtained to simplify data analysis. Figure 2 shows the distribution of the average standard deviations. The pseudorange ICB estimates for most stations were stable. Approximately 81 and 95 % of the stations had average standard deviations <0.25 and 0.35 m, respectively. Eight stations, including ADIS, KIS0 etc., had average standard deviations larger than 0.4 m. The maximum value (1.13 m) was achieved by OUS2. This result is probably caused by the gross errors in the GLONASS pseudorange observations from these stations.

The pseudorange ICB estimates remained stable over time when the firmware version or the antenna type was not changed. Thus, the average pseudorange ICB estimates were considered as the final results for each station to obtain more precise results.

Pseudorange ICBs for receivers with identical receiver firmware versions and antenna types

Wanninger (2012) found that GLONASS carrier phase ICB is related not only to receiver type but also to receiver firmware version and antenna type. Figure 1 shows that GLONASS pseudorange ICBs are closely related to receiver firmware version and antenna type. In this study, the relationship of pseudorange ICBs with receiver firmware version and antenna type was further studied.

Figure 3 shows the pseudorange ICB estimates of some selected stations equipped with the same firmware versions and antenna types. Their receiver types, firmware versions, and antenna types are listed in Table 3.

In general, the pseudorange ICB estimates corresponding to the same firmware versions and antenna types agreed well, except for station THTG. The standard deviations of pseudorange ICB estimates of all stations with the same firmware versions and antenna types were computed to assess the agreement among the pseudorange ICB estimates. Figure 4 shows the distribution of the standard deviations. Most standard deviations were <0.4 m, indicating good agreement in the pseudorange ICB estimates corresponding to the same firmware versions and antenna types among the stations. Therefore, these values were considered identical. In addition, some stations such as THTG had standard deviations larger than 0.4 m.

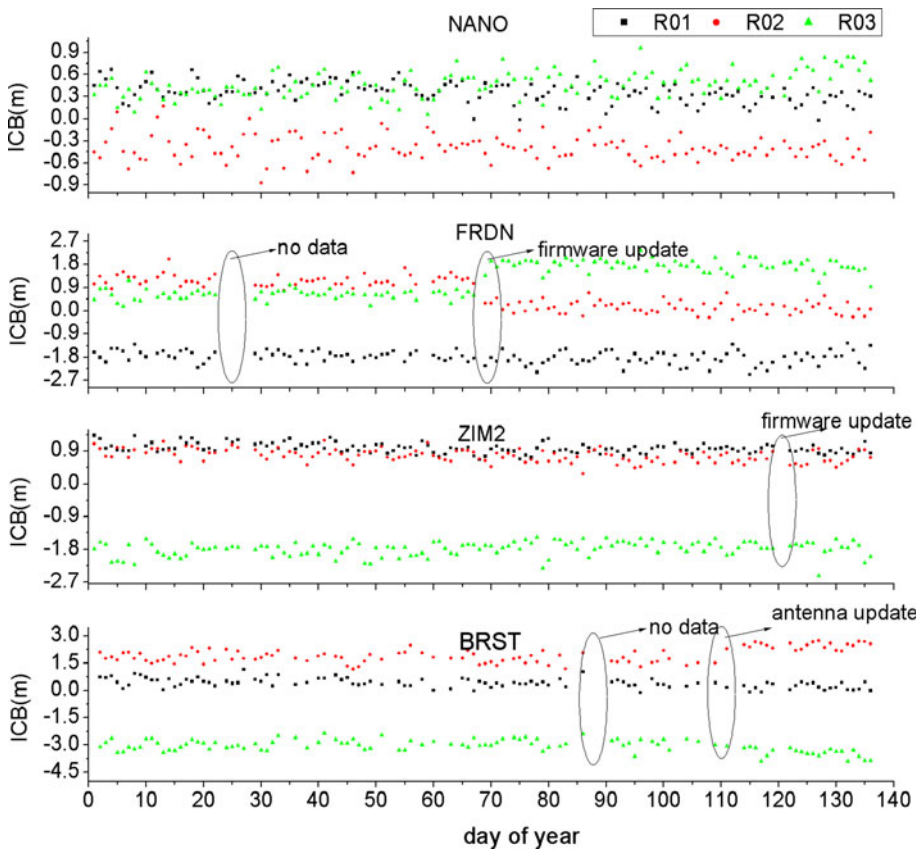

Fig. 1 Time series of the pseudorange ICB estimations at stations NANO, FRDN, ZIM2, and BRST

Table 2 Information on receiver types, firmware versions, and antenna types

Station	Receiver type	Antenna type	Firmware
NANO	Leica GRX1200GGPRO	LEIAT504GG	7.80
FRDN	TPS NETG3	TPSCR.G3	3.4/3.5
ZIM2	Trimble NetR5	TRM59800.00	4.43/4.48
BRST	Trimble NetR9	TRM55971.00/TRM57971.00	4.42

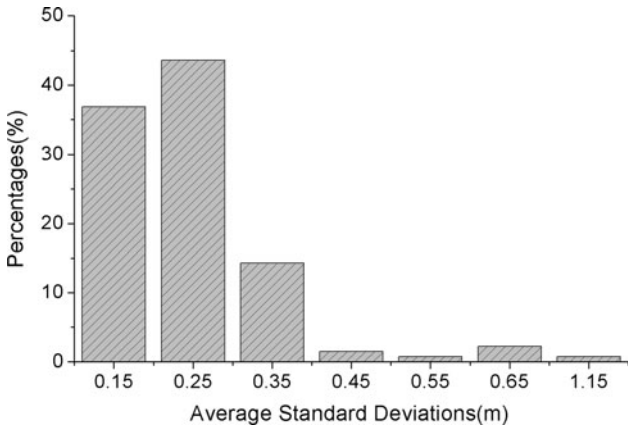

Fig. 2 Distribution of the average standard deviation of pseudorange ICBs for each station. For simplicity, the average standard deviation of 24 satellites was obtained for each station

Pseudorange ICBs for receivers with identical firmware versions but different antenna types

Figure 5 shows the pseudorange ICB estimates of selected stations equipped with the same firmware versions but different antenna types. The receiver types, firmware versions, and antenna types are listed in Table 4.

As shown in Fig. 5, the pseudorange ICB estimates of the stations with the same antenna types agreed well. However, stations DGAV, MOBJ, WARN, BDOS, WHIT, and IQAL with different antenna types had different ICB estimates, indicating that the variations may be caused by the different antenna types. Furthermore, we selected a reference station for each group and computed the ICB differences between the reference and other stations in the group. Figure 6 shows the relationship between the ICB differences and frequency.

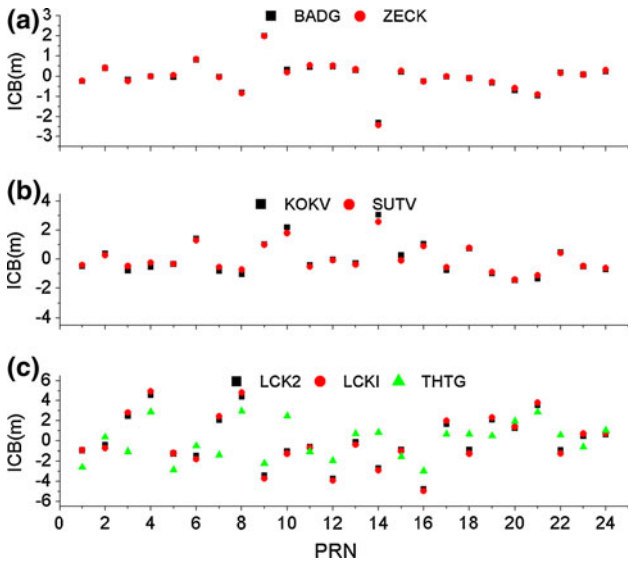

Fig. 3 Pseudorange ICB valuations of some stations selected from the stations equipped with the same firmware versions and antenna types

Table 3 Information on receiver types, firmware versions, and antenna types

Group	Receiver type	Antenna type	Firmware
a	Javad TRE_G3TH DELTA	JAVRINGANT_DM	3.2.7
b	Jps EGGDT	ASH701945G_M	2.7.0
c	Leica GRX1200 + GNSS	LEIAR25.R3	8.2

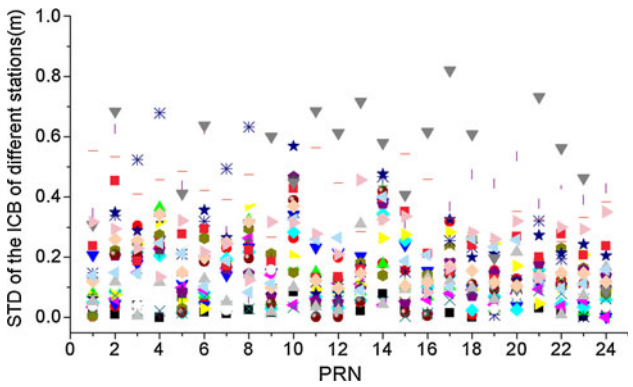

Fig. 4 Standard deviations of the pseudorange ICB estimates of all stations with the same firmware versions and antenna types. Each dot denotes a standard deviation for each satellite of a firmware version and antenna type

As shown in Fig. 6, the ICB differences of the satellites with the same frequency are almost equal. Moreover, the ICB differences among groups (a), (b), and (c) were approximately linear functions of frequency, but they exhibited different linear relationships for the positive and negative frequencies for group (d). Furthermore, the

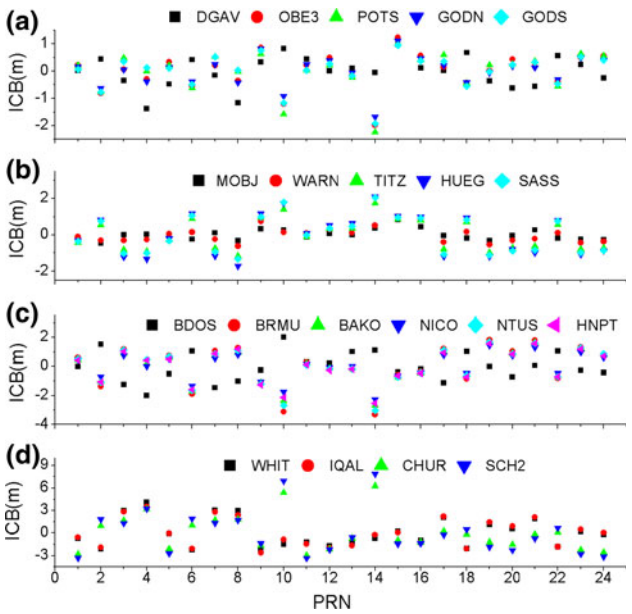

Fig. 5 Pseudorange ICB estimates of some stations selected from the stations equipped with the same firmware versions but different antennas. Group (**a**) is equipped with Javad TRE_G3TH DELTA, firmware version 3.35; Group (**b**) is equipped with Jps LEGACY, firmware version 2.6.1; Group (**c**) is equipped with Leica GRX1200GGPRO, firmware version 8.1; and Group (**d**) is equipped with Tps NET-G3A, firmware version 3.5

standard deviations of residuals fitted for most stations using the linear functions were <0.3 m. Thus, the ICB differences may be compensated with frequency function models. The standard deviations of the fitting residuals of all stations with the same firmware version were calculated after using frequency function models to show the feasibility of the method to compensate for the ICB differences. For simplicity, we used quadratic frequency function models for each firmware version group because of the different linear relationships of the ICB differences to the positive and negative frequencies for some stations. As shown in Fig. 7, over 80 % of the standard deviations were <0.4 m. This value represents the accuracy of pseudorange ICB estimations. Thus, this method is feasible.

These findings indicate that pseudorange ICB estimates with the same firmware versions have strong correlation. Although antenna types may cause obvious variations, the differences are closely related to frequency.

Pseudorange ICBs for receivers with different firmware versions

Given that pseudorange ICB valuations with the same firmware versions have strong correlation, we selected an antenna type as the reference and calibrated the differences caused by different antenna types. The average of the pseudorange ICB estimates of all stations with the same firmware versions was considered as the results of the firmware version. As shown in

Table 4 Antenna types of stations

Receiver type	Station name	Antenna type	Receiver type	Station name	Antenna type
JAVAD TRE_G3TH DELTA (3.3.5)	**DGAV**	**ASH701945E_M**	LEICA GRX1200 GGPRO (8.1)	**BDOS**	**ASH700936E_C**
	OBE3	JAV_RINGANT_G3T		BRMU	JAVRINGANT_DM
	POTS	JAV_RINGANT_G3T		BAKO	LEIAT504GG
	GODN	TPSCR.G3		NICO	LEIAT504GG
	GODS	TPSCR.G3		NTUS	LEIAT504GG
JPS LEGACY (2.6.1)	**MOBJ**	**JPSREGANT_SD_E**		HNPT	LEIAX1202GG
	WARN	**LEIAR25.R3**	TPS NET-G3A (3.5)	**WHIT**	**AOAD/M_T**
	TITZ	LEIAR25.R4		**IQAL**	**TPSCR.G3**
	HUEG	TPSCR3_GGD		CHUR	ASH701945E_M
	SASS	TPSCR3_GGD		SCH2	ASH701945E_M

The ICB results of some stations that vary with others in the same group are shown in bold

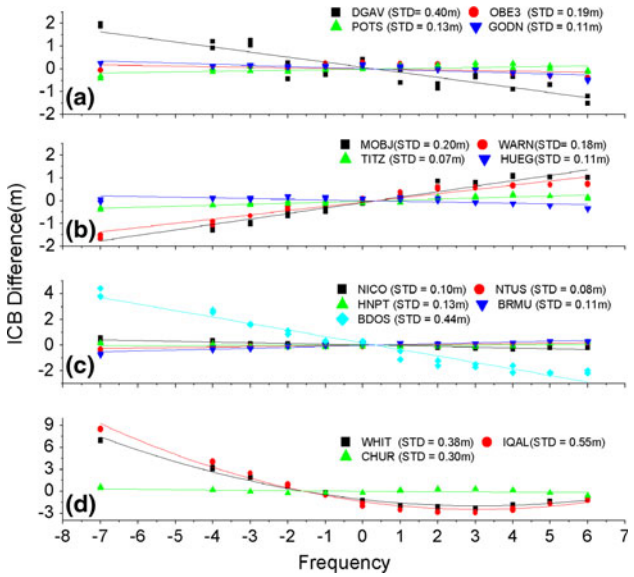

Fig. 6 Relationship between the ICB differences and frequency. The reference stations of Groups (**a**), (**b**), (**c**), and (**d**) are GODS, SASS, BAKO, and SCH2, respectively. The standard deviations of the fitting residuals for each station are shown on the right corner

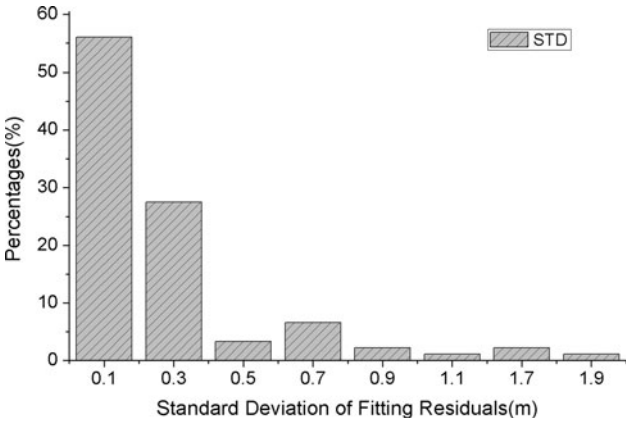

Fig. 7 Distribution of the standard deviations of the fitting residuals. For each firmware version group, we selected a reference station and then fitted the differences between the reference and other stations using frequency function models. For simplicity, we used quadratic frequency function models for each firmware version group because of the different linear relationships of the ICB differences to the positive and negative frequencies for some stations

Fig. 8, the pseudorange ICBs of Leica GRX1200GPRO receivers with firmware versions 7.8 and 8.1 agreed well, with a correlation coefficient of 0.99. However, the estimates for Javad TRE_G3TH DELTA receivers with firmware versions 3.35 and 3.2.7 as well as Trimble NetR9 receivers with firmware versions 4.17 and 4.42 showed evident variations, with correlation coefficients <0.5. Thus, given that pseudorange ICBs of different firmware versions are independent, they should be estimated independently.

Relationship between pseudorange ICBs and frequency

Al-Shaery et al. (2012) estimated double differenced pseudorange ICBs by assuming that these ICBs are linear functions of frequency. Thus, we analyzed whether undifferenced pseudorange ICBs are also linear functions of frequency. Figure 9 shows the relationships between undifferenced pseudorange ICBs and frequency. Moreover, we fit the pseudorange ICBs using linear frequency function models for Trimble NetR9 and Leica GRX1200GGPRO and quadratic frequency function models for Tps NET-G3A and Javad TRE_G3TH DELTA. As shown in Fig. 9, the pseudorange ICB valuations of the same frequency vary obviously, reaching more than 2 m for Javad TRE_G3TH DELTA. Furthermore, considerable fitting residuals were found for some satellites, and the standard deviations of fitting residuals were more than 0.4 m. Therefore, we suggest that pseudorange ICB valuations should be provided for each satellite to obtain more precise ICBs.

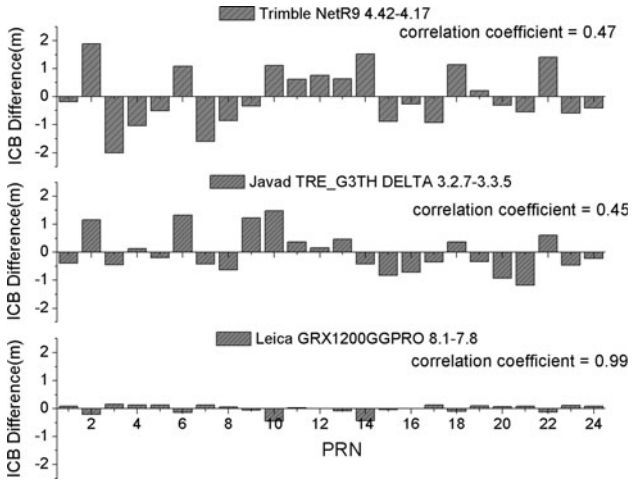

Fig. 8 Differences of pseudorange ICBs with different firmware versions. The correlation coefficients of the two groups of estimates are shown at the *top-right* corner

Calibration of pseudorange ICBs

GLONASS pseudorange ICB errors can reach up to several meters. Thus, they should be considered carefully. We compared the SPP solutions before and after the application of pseudorange ICB estimation. At the middle and low latitude areas, the number of visible GLONASS satellites is often below four within a day (Zheng et al. 2012) Thus, performing SPP over a whole day using only GLONASS measurements is impossible. To overcome this problem, we selected 26 individual stations at high latitude areas on January 10, 2012 (Fig. 10).

Results of SPP before and after pseudorange ICB calibration

Figures 11 and 12 show the time series of GLONASS SPP for station LAMA before and after pseudorange ICB calibration as well as their pseudorange posteriori residuals. As shown in Fig. 12, obvious systematic errors were present in the pseudorange posteriori residuals before pseudorange ICB calibration. Moreover, the systematic errors can reach up to several meters and vary for each satellite. Hence, the accuracy of GLONASS SPP without ICB calibration was very poor. However, the systematic errors were eliminated after pseudorange ICB calibration, thereby increasing the accuracy of GLONASS SPP. The RMS values of N, E, and U decreased from 1.73, 1.72, and 3.08 m to 0.44, 0.38, and 0.83 m, respectively.

Figure 13 shows the RMS of GPS and GLONASS before and after ICB calibration of SPP in the 26 individual stations. The positioning accuracy significantly improved after pseudorange ICB calibration. The mean RMS reduced from 2.02, 1.86, 4.44 m to 0.87, 0.97, 2.07 m in the East, North, and Up components, improving by 57, 48, and 53 %, respectively. When comparing to the solutions of GPS SPP, whose mean RMS reached 0.48, 0.75, 1.40 m in the East, North, and Up components, with pseudorange

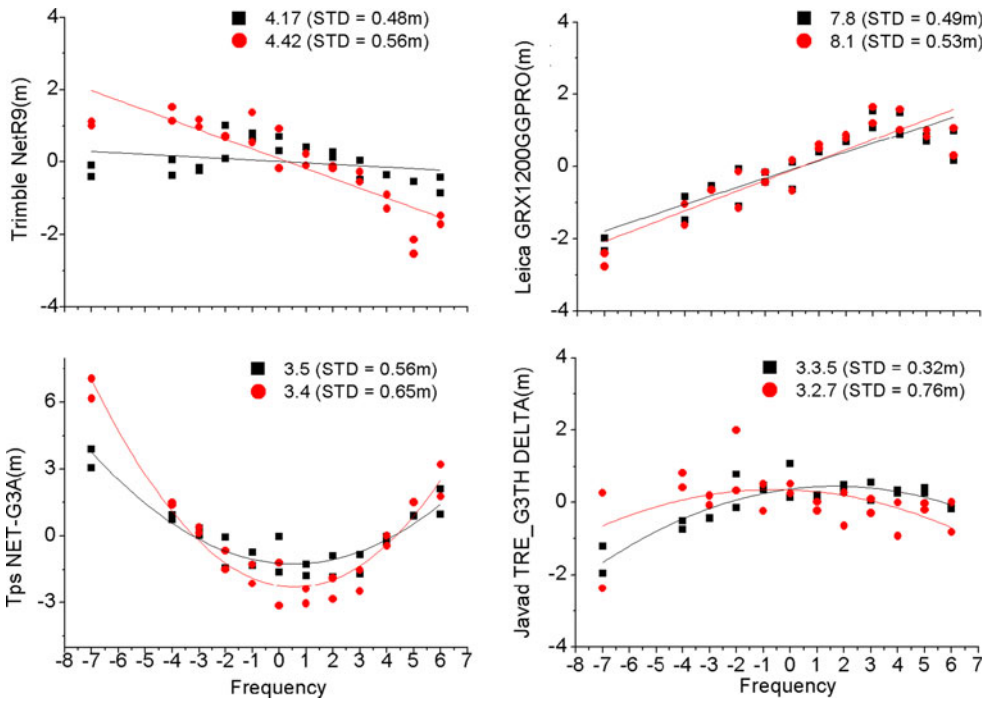

Fig. 9 Relationship between ICB evaluations and frequency. We fit the pseudorange ICBs using linear frequency function models for Trimble NetR9 and Leica GRX1200GGPRO, but quadratic frequency function models for Tps NET-G3A and Javad TRE_G3TH DELTA. The *fitted lines* and standard deviations of the fitting residuals are presented

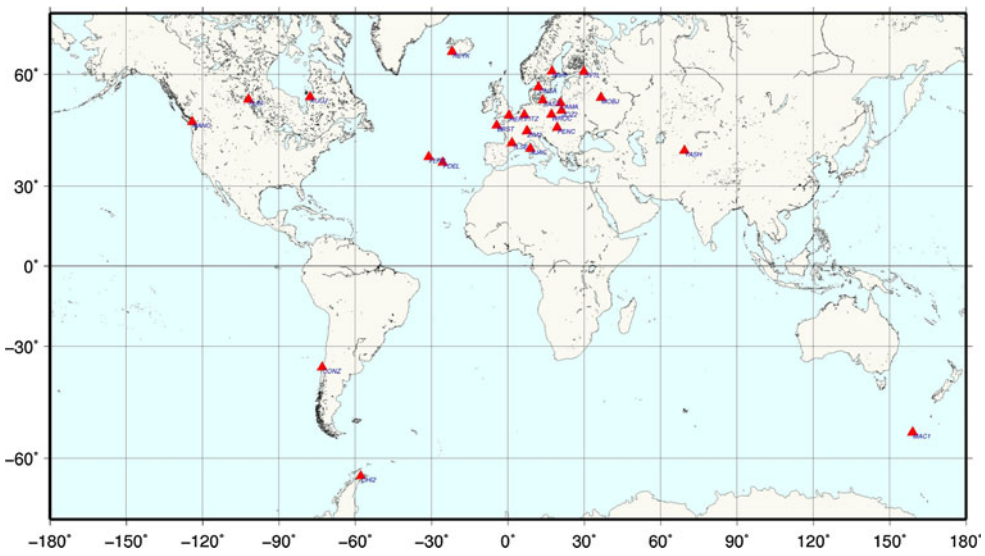

Fig. 10 Distribution of the 26 stations selected to test the applicability of pseudorange ICB estimates

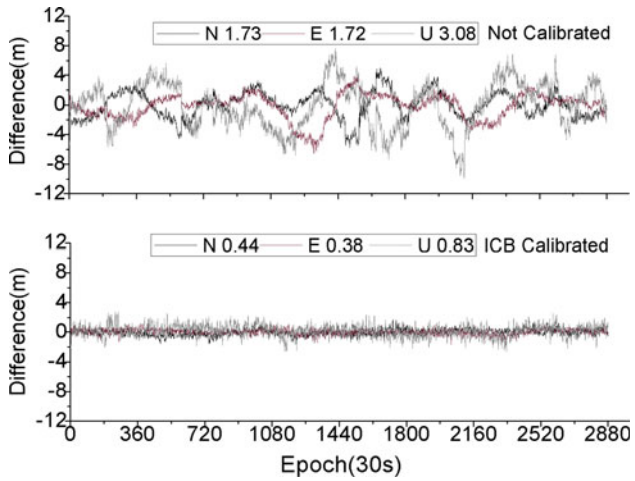

Fig. 11 Time series of the GLONASS SPP solutions for station LAMA on January 10, 2012

ICB calibration, the mean RMS of GLONASS SPP is still poor than that of GPS SPP. But for some individual stations, with pseudorange ICB calibration, GLONASS SPP can get the same accuracy level as GPS SPP.

Furthermore, we compared the solutions of GPS SPP and combined GPS/GLONASS SPP before and after pseudorange ICB calibration. Figure 14 shows the differences in RMS between GPS and combined GPS/GLONASS SPP before and after the pseudorange ICB calibration of the 26 stations. Compared with the solutions of GPS SPP, the improvements in combined GPS/GLONASS before the pseudorange ICB calibration in many stations were small. They were even worse for individual stations. However, after pseudorange ICB calibration, the RMS of combined GPS/GLONASS SPP was better than that of GPS SPP, with mean RMS improvements reaching 27, 17, and 23 % for the East, North, and Up components, respectively.

PPP convergence before and after pseudorange ICB calibration

At the initial convergence period, the accuracies of PPP are mainly determined by the accuracies of SPP because the carrier phase ambiguities have not yet been accurately determined (Geng et al. 2010a). In "Results of SPP before and after pseudorange ICB calibration" the RMS values of GLONASS SPP and combined GPS/GLONASS SPP improved after pseudorange ICB calibration. Thus, the convergence for PPP should also be accelerated. Figure 15 shows the time series of GPS PPP and combined GPS/GLONASS PPP before and after pseudorange ICB calibration. As the figure shows, GPS PPP required more convergence time. In addition, systematic biases of 15 and 10 cm were found in the East and Up components after 15 min convergence, respectively, resulting in the reduction of more time (here approximately 40 min). The result of combined GPS/GLONASS PPP was better than that of GPS PPP because it involved more observations and stronger geometry of satellites. However, the GLONASS pseudorange observations may have several meters of systematic errors before pseudorange ICB calibration. Thus, the results of the East and Up components of the combined GPS/GLONASS PPP were worse than those of GPS PPP during the initialization phase. After pseudorange ICB calibration, the results for the North, East, and Up components were all better than the GPS-derived results.

Figure 16 shows the distribution of the RMS of GPS PPP and combined GPS/GLONASS PPP before and after pseudorange ICB calibration after 10, 15, 20, and 30 min convergence. The 24 h data of 26 individual stations were divided into 10, 15, 20, and 30 min to enlarge the data samples. The mean RMS values of GPS PPP after 10, 15,

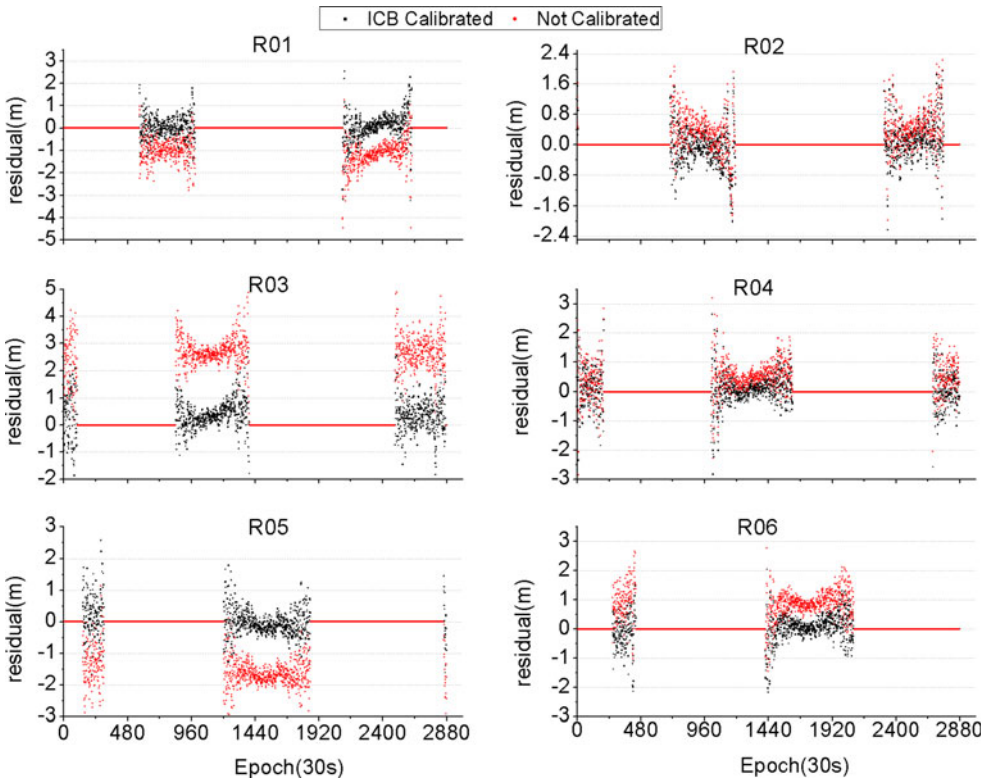

Fig. 12 GLONASS SPP Pseudorange posteriori residuals of satellites R01 to R06

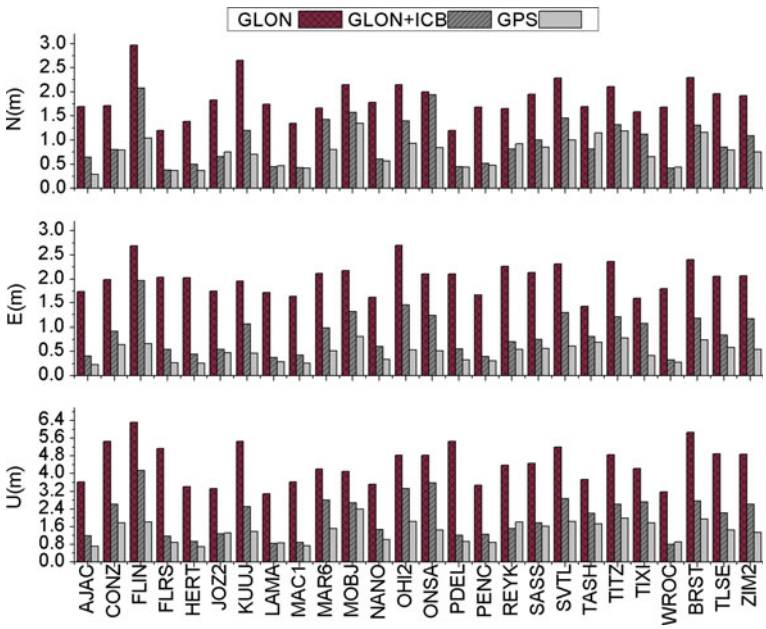

Fig. 13 RMS of GPS and GLONASS before and after the ICB calibration of SPP at all stations

20, and 30 min convergence were 0.40, 0.32, 0.26, and 0.18 m, with maximum RMS values of 2.89, 1.83, 1.95, and 1.15 m, respectively. By contrast, the mean RMS values of combined GPS/GLONASS reduced to 0.28, 0.18, 0.13, and 0.08 m, with maximum RMS values of 1.16, 0.90, 0.84, and 0.83 m, respectively. Combined GPS/GLONASS PPP evidently improved the convergence speed, and the mean RMS of PPP improved by almost 50 % during the convergence period. After pseudorange ICB calibrations, the convergence speed can be further improved. The mean RMS values further reduced to 0.22, 0.14, 0.11, and 0.07 m, respectively.

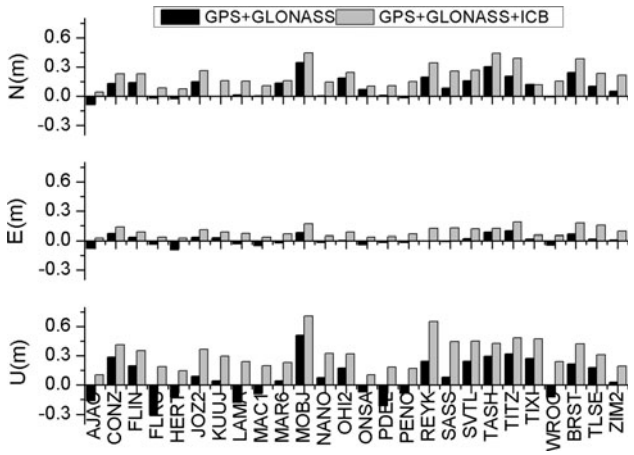

Fig. 14 RMS of GPS SPP minus the RMS of combined GPS/GLONASS SPP before and after pseudorange ICB calibration. The weight ratio of GLONASS and GPS measurements in the least-squares adjustment is set as 1:2. Positive values mean the GPS + GLON rms < GPS rms

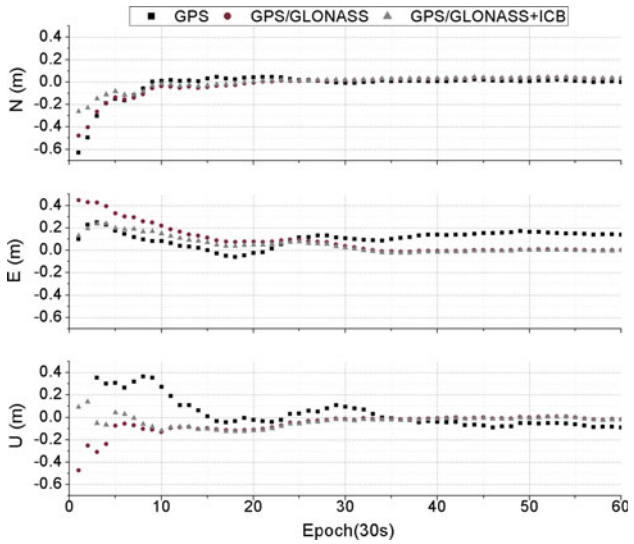

Fig. 15 Time series of the convergence period of GPS PPP and combined GPS/GLONASS PPP before and after pseudorange ICB calibration in station LAMA. The weight ratio of GLONASS and GPS measurements in the Kalman filter is set as 1:2

GLONASS observations are important in combined GPS/GLONASS PPP when tracking only a few GPS satellites. Thus, we also discussed the contribution of the pseudorange ICBs on GLONASS PPP. Figure 17 shows the RMS distribution of GLONASS PPP before and after pseudorange ICB calibration after 10, 15, 20, and 30 min convergence. Before pseudorange ICB calibration, the mean RMS can reach up to 1.33 m, and the maximum RMS could even reach up to 13.26 m after 30 min convergence. However, the mean RMS decreased to 0.36 m, and the maximum RMS decreased to 2.78 m. The pseudorange ICB calibration not only significantly improved the accuracy of GLONASS SPP but also benefitted the determination of ambiguities.

Conclusions

In this study, we estimated the GLONASS undifferenced pseudorange ICBs for 133 individual GPS/GLONASS receivers produced by five manufacturers. The following conclusions could be drawn from the results. First, GLONASS pseudorange ICBs remain stable over time. Second, pseudorange ICBs of stations with the same firmware version are strongly correlated. Although different antenna types can cause different pseudorange ICBs, the variances have close relationships with frequency. Third, pseudorange ICBs with different firmware versions vary and have little correlation. Fourth, pseudorange ICBs should be provided for each satellite to obtain more precise ICBs. Fifth, pseudorange ICB calibration improves the mean RMS of GLONASS SPP by 57, 48, and 53 % for the East, North, and Up components, respectively. The mean RMS improvement of combined GPS/GLONASS SPP reaches up to 27, 17, and 23 % compared with that of GPS SPP. Finally, pseudorange ICB calibration significantly improves the convergence speed of GLONASS and combined GPS/GLONASS PPP.

Organizations such as IGS are recommended to provide pseudorange ICB products for GLONASS pseudorange ICB calibration. These products should contain the ICB calibrations of each GLONASS satellite based on the

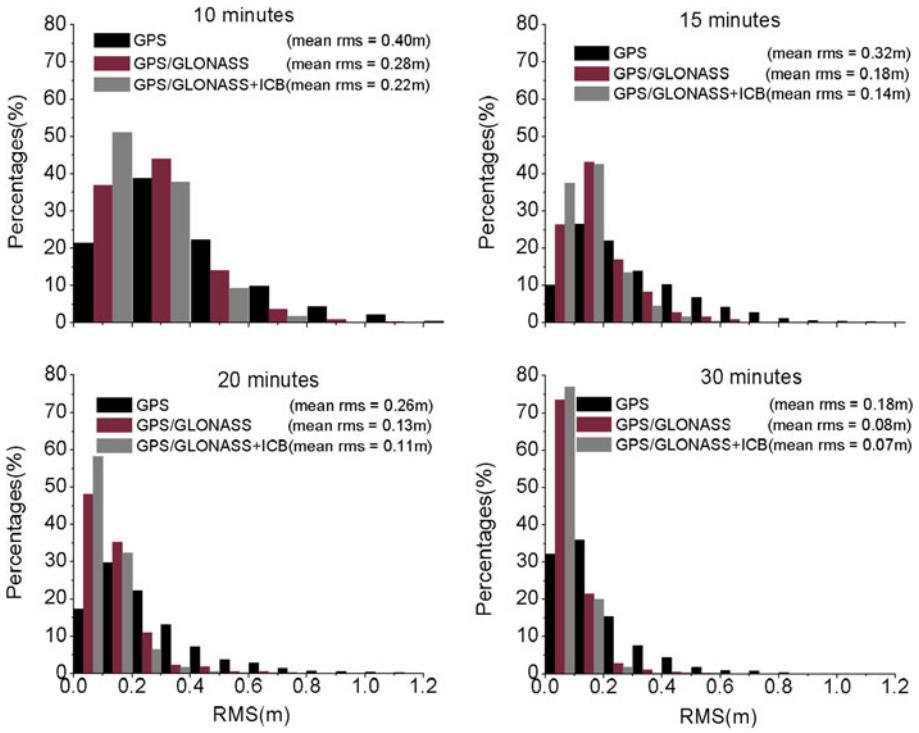

Fig. 16 Distribution of the RMS of GPS PPP and combined GPS/GLONASS PPP before and after pseudorange ICB calibration after 10, 15, 20, and 30 min convergence. The RMS of the results of the last 2 min was calculated for each data sample, and the mean RMS for each group is also shown. The weight ratio of GLONASS and GPS measurements in the Kalman filter is set as 1:2

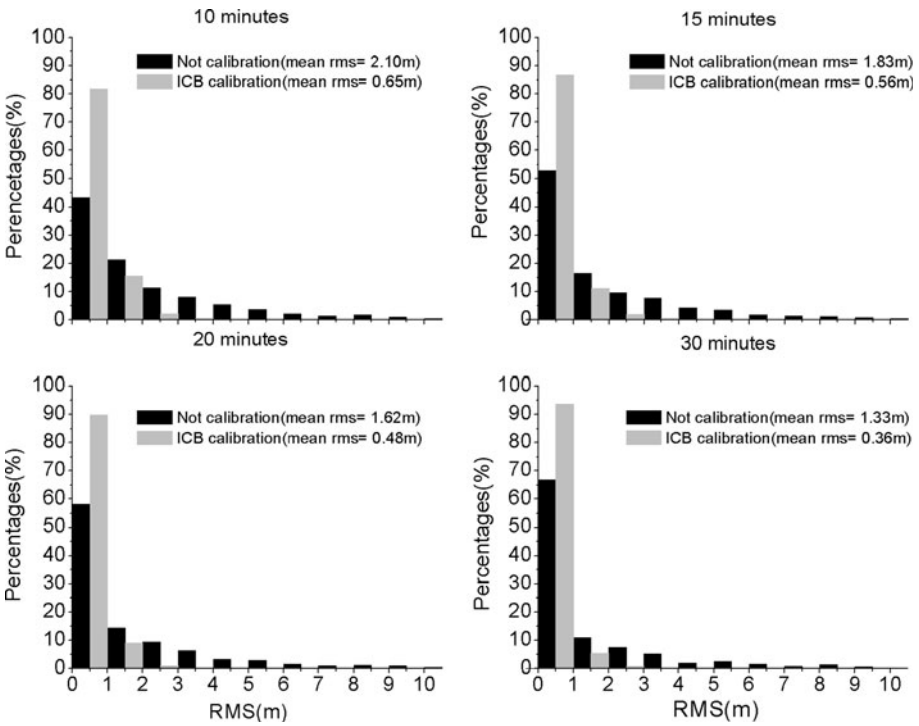

Fig. 17 Distribution of the RMS of GLONASS PPP before and after pseudorange ICB calibration after 10, 15, 20, and 30 min convergence. The data samples are the same as those in Fig. 16

receiver type and firmware version. PPP users can use these products to calibrate GLONASS pseudorange ICB errors and estimate the uncalibrated portions caused by different antenna types using quadratic function models.

Acknowledgments We thank Dr. Jianghui Geng, at University of California San Diego, for his valuable suggestions on this study. This study was supported by the National High Technology Research and Development Program of China (863 Program) (Grant No.2012AA12 A202), China Postdoctoral Science Foundation (Grant No.2012M51

1671) and also by the Fundamental Research Funds for the Central Universities (Grant No.2012618020202).

References

Al-Shaery A, Zhang S, Rizos C (2012) An enhanced calibration method of GLONASS inter-channel bias for GNSS RTK. GPS Solut 2012(1):1–9

Bisnath S, Gao Y (2008) Current state of precise point positioning and future prospects and limitations. In: Sideris MG (ed) Observing our changing earth. Springer, New York, pp 615–623

Ge M, Gendt G, Rothacher M, Shi C, Liu J (2008) Resolution of GPS carrier phase ambiguities in precise point positioning (PPP) with daily observations. J Geod 82(7):389–399

Geng J, Meng X, Dodson AH, Ge M, Teferle FN (2010a) Rapid re-convergences to ambiguity-fixed solutions in precise point positioning. J Geod 84(12):705–714

Geng J, Meng X, Dodson AH, Teferle FN (2010b) Integer ambiguity resolution in precise point positioning: method comparison. J Geod 84(9):569–581

Geng J, Shi C, Ge M, Dodson AH, Lou Y, Zhao Q, Liu J (2012) Improving the estimation of fractional-cycle biases for ambiguity resolution in precise point positioning. J Geod 86(8):579–589

Kozlov D, Tkachenko M (1998) Centimeter-level, real-time kinematic positioning with GPS + GLONASS C/A receivers. Navigation 45(2):137–147

Kozlov D, Tkachenko M, Tochilin A (2000) Statistical characterization of hardware biases in GPS + GLONASS receivers. In: proceedings of ION GPS-2000. US Institution of Navigation, Salt Lake City, Utah, pp 817–826

Leos Mervart, Georg Weber (2011) Real-time combination of GNSS orbit and clock correction streams using a Kalman filter approach. In: proceedings of ION GNSS-2011. Institute of Navigation, Portland OR, pp 707–711

Rossbach U, Hein G (1996) Treatment of integer ambiguities in DGPS/DGLONASS double difference carrier phase solution. In: proceedings ION GPS-1996. Institute of Navigation, Kansas City, MO, pp 909–916

Tsujii T, Harigae M, Inagaki T (2000) Flight tests of GPS/GLONASS precise positioning versus dual frequency KGPS profile. Earth Planet Space 52:825–829

Wanninger L (2012) Carrier phase inter-frequency biases of GLONASS receivers. J Geod 86(2):139–148

Wanninger L, Wallstab-Freitag S (2007) Combined processing of GPS,GLONASS, and SBAS code phase and carrier phase measurements. In: proceedings of ION GNSS-2007. Institution of Navigation, Fort Worth, Texas, pp 866–875

Yamanda H, Takasu T, Kubo N, Yasuda A (2010) Evaluation and calibration of receiver inter-channel biases for RTK-GPS/GLONASS. In: proceedings of ION GNSS-2010. Institute of Navigation, Portland, Oregon, pp 1580–1587

Zheng Y, Nie G, Fang R, Yin Q, Yi W, Liu J (2012) Investigation of GLONASS performance in differential positioning. Earth Sci Inform 5(3–4):189–199

Zinoviev AE (2005) Using GLONASS in combined GNSS receivers: current status. In: proceedings of ION GNSS-2005. Institution of Navigation, Long Beach, California, pp 1046–1057

Zumberge JF, Heflin MB, Jefferson DC, Watkins MM, Webb FH (1997) Precise point positioning for the efficient and robust analysis of GPS data from large networks. J Geophys Res 102(B3):5005–5017

Author Biographies

Shi Chuang is the head for GNSS Research Center of Wuhan University. He graduated from Wuhan University and obtained his Ph.D. degree in 1998. His research interests include network adjustment, precise orbit determination of GNSS satellites and LEOs and real-time precise point positioning (PPP).

Yi Wenting is currently a Ph.D. student at the Wuhan University. He has obtained his Bachelor's degree from Wuhan University, P.R.C. in 2009. His current research focuses mainly involve GNSS precise positioning technology.

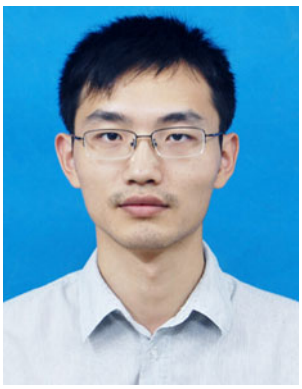

Song Weiwei is currently a post doctorate fellow at the Wuhan University. He has obtained his Ph.D. degree from Wuhan University, P.R.C., in 2011. His current research mainly focuses on real-time GNSS precise positioning technology.

Lou Yidong is currently an Associate Professor at GNSS Research Center, Wuhan University. He obtained his Ph.D. in Geodesy and Surveying Engineering from the Wuhan University in 2008. His current research interest is in the real-time precise GNSS Orbit determination and real-time GNSS precise point positioning. He is one of the members who have developed the PANDA software which has been widely used in china.

Yao Yibin is currently a professor at the Wuhan University. He obtained his B.Sc., Master, and Ph.D. degrees with distinction in Geodesy and Surveying Engineering at the School of Geodesy and Geomatics in Wuhan University in 1997, 2000, and 2004. His main research interests include GPS/MET and high-precision GPS data processing.

Zhang Rui is currently a Ph.D. student at the Wuhan University. She has obtained her Master's degree from Wuhan University, P.R.C. in 2010. Her current research focuses mainly involve GNSS precise positioning technology, GNSS meteorology etc.